INFLUENCE OF ICE THICKNESS ON SMOS AND AQUARIUS BRIGHTNESS TEMPERATURES OVER ANTARCTICA

M. Pablos[1,3], *M. Piles*[1,3], *V. González-Gambau*[2,3], *A. Camps*[1,3], *M. Vall-llossera*[1,3]

[1]Universitat Politècnica de Catalunya and IEEC/UPC, Jordi Girona 1-3, 08034 Barcelona, Spain
[2]Institut de Ciències del Mar/CSIC, Pg. Marítim Barceloneta 37-49, 08003 Barcelona, Spain
[3]SMOS Barcelona Expert Centre, Pg. Marítim Barceloneta 37-49, 08003 Barcelona, Spain
E-mail: miriam.pablos@tsc.upc.edu

ABSTRACT

The Dome-C region, in the East Antarctic Plateau, has been used for calibration/validation of satellite microwave radiometers since the 1970's. However, its use as an independent external target has been recently questioned due to some spatial inhomogeneities found in L-band airborne and satellite observations.

This work evidences the influence of the Antarctic ice thickness spatial variations on the measured SMOS and Aquarius brightness temperatures (T_B). The possible effects of subglacial water and bedrock on the acquired radiometric signals have also been analyzed. A 3-months no-daylight period during the Austral winter has been selected. Four transects over East Antarctica have been defined to study the spatial variations. A good agreement between SMOS and Aquarius T_B changes and ice thickness variations over the whole Antarctica has been observed, obtaining linear correlations of 0.6–0.7 and slopes of 8.6–9.5 K/km. The subglacial lakes may affect the vertical physical temperature profile and/or the dielectric properties of the ice layers above. As expected, the subglacial bedrock is not contributing to the measured T_B, since the maximum estimated L-band penetration depth is $\sim$1–1.5 km.

Index Terms— Ice thickness, subglacial lakes, subglacial bedrock, Antarctica, brightness temperature, L-band radiometer, SMOS, Aquarius.

1. INTRODUCTION

The Soil Moisture and Ocean Salinity (SMOS) mission from the European Space Agency (ESA) was launched on November 2, 2009, to provide for the first time global observations of soil moisture (SM) and sea surface salinity (SSS). Its payload is a novel interferometric L-band radiometer, the Microwave Imaging Radiometer with Aperture Synthesis (MIRAS). It has full-polarization capabilities measuring all the four Stokes parameters and provides multi-angular observations (from 0° to 65°) with a spatial resolution of $\sim$35–50 km.

The Aquarius/SAC-D mission, devoted to monitor the global SSS, was launched on June 10, 2011, as a collaboration between the U.S. National Aeronautics and Space Administration (NASA), and the Argentinian *COmisión Nacional de Actividades Espaciales* (CONAE). Aquarius carries on-board three L-band real aperture radiometers/scatterometers feeded by the same reflector, in a push-broom configuration at three incidence angles (29.36°, 38.49° and 46.29° for the inner, middle and outer beams, respetively), measuring the first, the second and the third Stokes parameters with $\sim$100 km of spatial resolution.

Although these two missions were planned for SM and/or SSS observations, their orbits allow to collect a large number of measurements in the polar regions. Also, it is known that microwave observations are affected by different physical ice characteristics, such as snow density, temperature, grain size, liquid water content, etc, and their variations along depth. It is anticipated that SMOS and Aquarius continuous polar views at L-band could provide new useful information to cryospheric studies.

The Dome-C region, in the East Antarctic Plateau, has been used as an independent external target for calibration/validation of satellite microwave radiometers since the 1970's. At L-band, the thermal stability of this region has been confirmed by several experimental campaigns [1, 2]. However, recent studies using L-band airborne and satellite observations have revealed some spatial inhomogeneities [3, 4] and seasonal effects [4] in the acquired brightness temperatures (T_B) over this area.

This paper explores the influence of the Antarctic ice thickness on the spatial variations of SMOS and Aquarius T_B over Antarctica.

2. DATA AND METHODOLOGY

The SMOS T_B at the antenna plane are obtained from the L1C V5.05 products. They have been screened out for all Radio Frequency Interferences (RFIs) detected (strong, point source and tails), Sun (glint area, aliases and tails) and Moon (aliases) contamination, using the flags provided with the products. Later, the geometric and Faraday corrections are applied to obtain T_B at the Top Of the Atmosphere (TOA). The measured SMOS T_B are interpolated to the Aquarius incidence angles (θ_i) in a range of $\theta_i \pm 5°$.

The Aquarius T_B at TOA are obtained from the L2 V3.0 products. They have been masked out for all Aquarius maneuvers, RFI, Sun reflected, glint, and Moon (using the moderate and severe flags) and Sun directed (using the severe flag).

A gridding procedure has been applied to the data of both instruments. The spatial sampling has been selected to fulfill the Nyquist criterium according to the spatial resolution of each radiometer. SMOS T_B have been projected from the Icosahedral Snyder Equal Area (ISEA) 4H9 gridpoints to a 25-km Equal Area Scalable Earth (EASE) grid. The Aquarius T_B have been first projected to a 50-km EASE grid, using the coordinates of the center and the edges of each footprint. Secondly, they have been resampled to the same grid as SMOS using a nearest-neighbour approach. The sea area around the Antarctic continent has been removed to have only measurements over the continental ice sheet. Aquarius tracks produce a larger area

The work presented in this paper was supported by the Spanish Ministry of Economy and Competitiveness, with a Formación Personal de Investigación (FPI) grant BES-2011-043322, the project MIDAS 7: AYA2012-39356-C05, and ERDF (European Regional Development Fund).

without data at the South Pole, but the same unobserved region has been considered both for SMOS and Aquarius. Also, coastal areas over land (∼150 km) have been filtered to avoid the land-sea contamination effect.

Three additional datasets have been used: (i) the surface temperature in a 0.125° regular grid over the Antarctica, from the European Centre for Medium-Range Weather Forecasts (ECMWF), (ii) the subglacial bedrock elevation and the ice thickness in a 1-km regular grid, provided by the Bedmap2 project [5], and (iii) the most recent inventory of 379 Antarctic subglacial lakes [6]. These datasets have also been projected to the same 25-km EASE grid.

To minimize the impact of surface temperature changes on T_B variations, both ascending and descending SMOS and Aquarius orbits during a 3-months no-daylight period at latitudes below 65°S for all possible longitudes have been selected (from May 6 to August 6, 2013). All observations from this period are averaged to obtain maps for each beam at horizontal (H) and vertical (V) polarizations. Half of the First Stokes parameter ($I2$), computed from the T_B at TOA in this way: $I2 = (T_{B_H} + T_{B_V})/2$, has been used to avoid possible errors due to Faraday corrections.

The ECMWF surface temperature over Antarctica has been analyzed. The mean and the standard deviation (std) for the entire year 2013 and for the selected no-daylight period are shown in Fig. 1. Note that the spatial pattern of the mean surface temperature is similar in both periods. As expected, the surface temperature is colder during the no-daylight period and its variability is lower (higher std during 2013 than at no-daylight period). Therefore, the no-daylight period is used in this study to safely assume that T_B variations are not due to surface temperature variations.

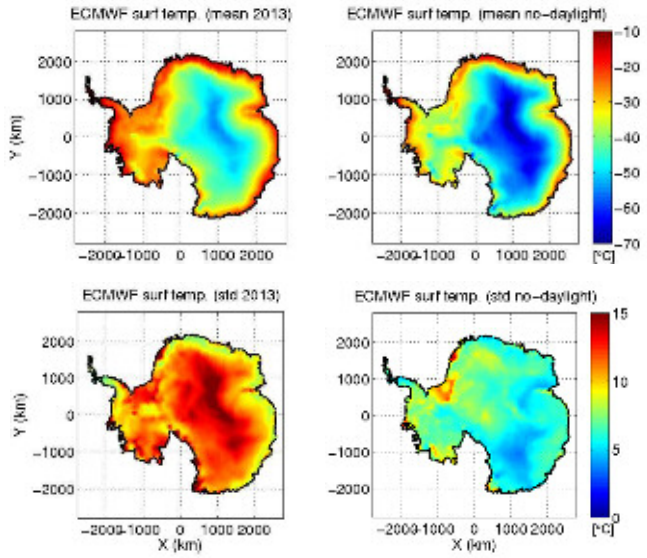

Fig. 1. ECMWF surface temperature over Antarctica. Mean (top) and std (bottom) during 2013 (left) and no-daylight period (right).

The Antarctic datasets (subglacial bedrock and ice thickness) are displayed in Fig. 2. The bedrock varies from -2.2 km below to 2.2 km above the WGS-84 sea level and it could be positive or negative. The ice thickness, referred to the ice surface with positive axis defined upwards, called hereafter ice thickness level (IceTL), varies from 0 km (at the coast) to -4.3 km (around Dome-C area) and is always negative. Also, a map showing the pixels including at least one of the reported subglacial lakes as well as the selected transects for the analysis is included.

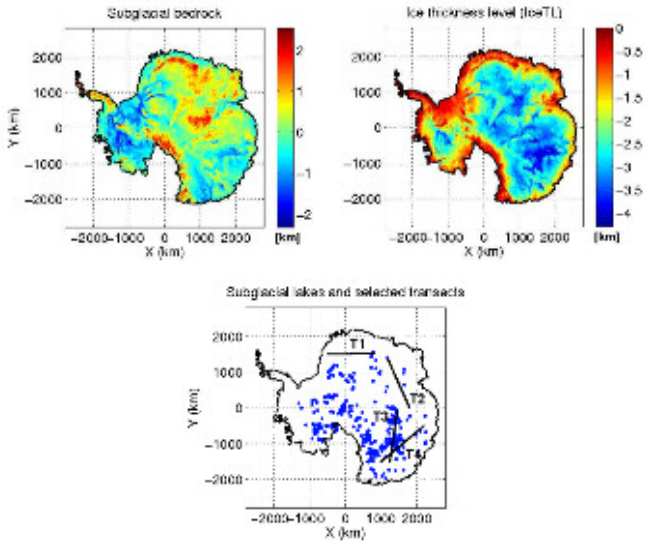

Fig. 2. Subglacial bedrock referred to WGS-84 (top left), ice thickness referred to surface level (top right), and map of subglacial lakes and selected transects (bottom).

3. RESULTS

A theoretical estimation of the L-band penetration depth has been used to investigate the role of the different possible contributions to the observed signal. It has been computed as follows: $\delta_p = \frac{\lambda\sqrt{\epsilon'}}{2\pi\epsilon''}$, where λ corresponds to the wavelength, ϵ' is the permittivity, and ϵ'' is the loss factor. For a constant frequency (1.413 GHz), the lowest physical temperature is associated to the lowest ϵ'' and, consequently, to the largest δ_p. An ice-air mixture model for spherical inclusions has been used [7]. It takes into account that the density of the Antarctic ice sheet increases exponentially with depth [8]. Also, the physical temperature from the surface to the bedrock has an exponential profile that increases with depth [9], using: ice surface temperature (-70°C, from ECMWF), geothermal heat flux (47 mW/m^2), ice thermal conductivity (2.7 W/mK), ice thermal diffusivity (45 m^2/yr), ice thickness (4300 m, from [5]), and accumulation rate (0.03 m/yr, from [1]). A more complex formulation would be needed to include the fluctuation effects of snow density and grain size, which are not considered in this work. The predicted δ_p as a function of depth is shown in Fig. 3. Its corresponding ϵ'' for each δ_p value is included inside. It can be observed that δ_p quickly decreases in the first 100 m. The reason for this decrease is the fast increase of the ice density. Then, the maximum δ_p is estimated to be ∼1–1.5 km. This suggests that the subglacial bedrock is not contributing to the observed T_B, since it lies deeper (∼2–4.3 km below the ice surface, except in the coastal areas), specially at the East Antarctic Plateau.

The mean and std Aquarius and SMOS $I2$ maps over Antarctica (middle beam) for the no-daylight study period are shown in Fig. 4. In both instruments, the mean $I2$ presents the warmer values at the coastal areas and colder values over the East Antarctic Plateau. Note that Aquarius $I2$ are slightly higher than SMOS $I2$,

in agreement with previous studies [4]. In general, areas with subglacial lakes (see Fig. 2 bottom) correspond to areas with the lowest observed $I2$ values. In the std, Aquarius shows lower values than SMOS. This is consistent with their instrument type. Aquarius is a real aperture radiometer whereas SMOS is a synthetic aperture radiometer, inherently noisier due to the image reconstruction procedure. The Aquarius std map has some features of significantly high values, particularly in the coastal areas, that are not present in SMOS. This may be an effect produced by the abrupt ice surface changes due to the strong topography that is above the mean std. In the SMOS std map, the different number of observations averaged per cell is responsable for the non-geophysical circular artifact with high std values.

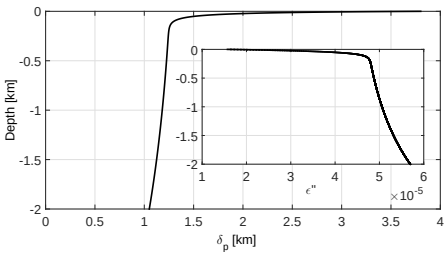

Fig. 3. Theoretical L-band penetration depth using the ice-air mixture model, and the vertical ice density and physical temperature profiles. Its corresponding ϵ'' is included inside.

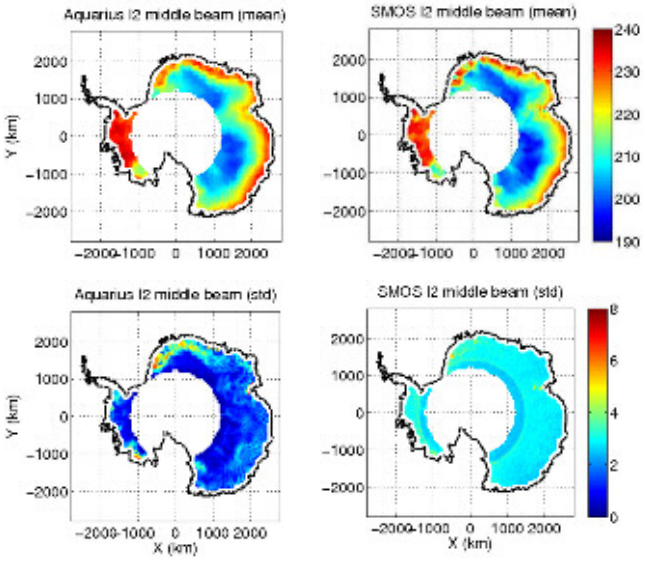

Fig. 4. Mean (top) and std (bottom) of Aquarius (left) and SMOS $I2$ (right) during the no-daylight period using the middle beam.

Aquarius and SMOS $I2$ variations ($\Delta I2 = I2 - \overline{I2}$) for the middle beam along the four transects, and the IceTL are shown in Fig. 5. Their corresponding mean value ($\overline{I2}$) is included in the legends and has been substracted to the actual values to better compare Aquarius and SMOS in the same plot. Note that the $I2$ changes of both instruments follow the overall trend of the IceTL variations in all transects, and a very close agreement can be observed when IceTL presents slow variations in space, as occurs in T1. In the other transects, the agreement is limited when IceTL exhibits fast spatial variations that cannot be resolved by Aquarius and SMOS. Nevertheless, SMOS $I2$ has a better agreement with the IceTL variations than Aquarius $I2$, which can be explained by its higher spatial resolution. In addition, T3 and T4 have the highest presence of known subglacial lakes (see Fig. 2 bottom). We hypothesize that the subglacial lakes and possible water connections between them may have an influence on the vertical physical temperature profile, and consequently, modify the dielectric properties and the emissivity of the ice layers overlaying these lakes.

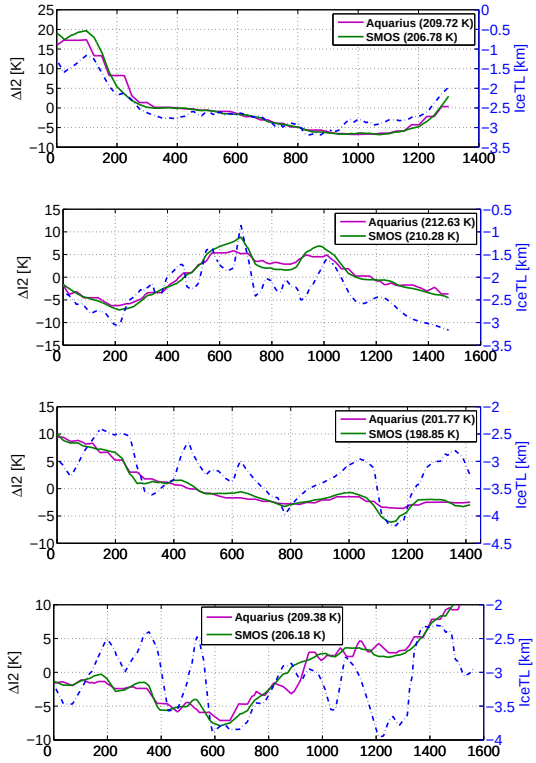

Fig. 5. Aquarius (magenta solid line) and SMOS (green solid line) $I2$ variations ($\Delta I2 = I2 - \overline{I2}$) for the middle beam, and ice thickness level (blue dashed line) along the four transects. Legends display $\overline{I2}$ values subtracted.

Correlations between Aquarius or SMOS $I2$ and subglacial bedrock (R_b), and IceTL (R_i), and slope between Aquarius or SMOS $I2$ and IceTL (s_i) for all pixels in the map are summarized in Table 1. Statistics with IceTL are also displayed separately for the pixels with known subglacial lakes and for a representative selection of a comparable number of pixels without subglacial lakes. All statistical scores are significant (p<0.05). As expected considering the predicted δ_p, no correlation has been observed with the subglacial bedrock ($R_b \approx$0.07 to 0.22). Correlations with IceTL are $R_i \approx$0.64 to 0.70. Slopes indicate there is a sensitivity of $\sim$8.6–9.5 K/km to variations in IceTL. The presence of subglacial water does not have an important impact in the correlations. However, lower slopes are obtained considering the pixels with known subglacial lakes in both instruments. The estimated errors in the slopes are higher than when all pixels are considered due to the reduced number of data points ($\sim$170 pixels), but remain within reasonable bounds. Results obtai-

Table 1. Correlation between Aquarius or SMOS $I2$ and subglacial bedrock (R_b), and IceTL (R_i), and slope between Aquarius or SMOS $I2$ and IceTL (s_i) for all pixels in the map. Statistics with IceTL are also displayed separately for the pixels with known subglacial lakes and for a representative selection of a comparable number of pixels without subglacial lakes. All statistical scores are significant ($p<0.05$).

Radiometer	Beam	All pixels			Pixels with lakes		Pixels without lakes	
		R_b	R_i	s_i [K/km]	R_i	s_i [K/km]	R_i	s_i [K/km]
Aquarius	inner	0.22	0.64	8.9 ± 0.1	0.67	7.5 ± 0.5	0.69	9.3 ± 0.7
	middle	0.18	0.65	9.0 ± 0.1	0.68	6.1 ± 0.5	0.71	9.3 ± 0.7
	outer	0.11	0.66	8.6 ± 0.1	0.65	6.0 ± 0.5	0.73	9.8 ± 0.7
SMOS	inner	0.19	0.65	9.3 ± 0.1	0.68	7.9 ± 0.5	0.69	9.6 ± 0.7
	middle	0.16	0.68	9.5 ± 0.1	0.70	6.1 ± 0.4	0.72	9.6 ± 0.7
	outer	0.07	0.70	9.3 ± 0.1	0.69	5.8 ± 0.4	0.75	10.0 ± 0.7

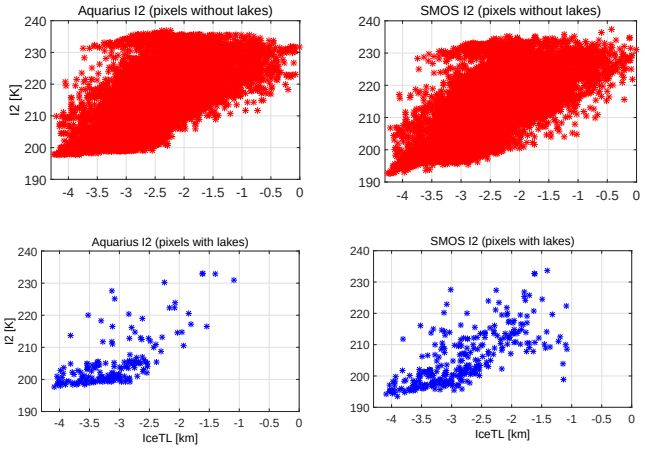

Fig. 6. Aquarius (left) and SMOS $I2$ (right) during the no-daylight period using the middle beam *vs.* Antarctic ice thickness for pixels without known lakes (top) and for pixels with known lakes (bottom).

ned with Aquarius are very similar to those obtained with SMOS. Also, similar results and statistics are obtained at H and V polarization, and using the other beams.

Scatter plots of Aquarius and SMOS $I2$ (middle beam) vs Antarctic IceTL are presented in Fig. 6 for the pixels without and with reported subglacial lakes. A linear relationship can be distinguished for the two distributions and for the two instruments. Also, it can be observed that the pixels with subglacial lakes are, in general, concentrated in the lower values of $I2$, specially for Aquarius. This seems to indicate that the presence of water underneath the ice influences the measured $I2$.

4. CONCLUSIONS

In this study, the influence of Antarctic ice thickness spatial variations in measured Aquarius and SMOS $I2$ is analyzed. Austral winter conditions (a 3-months no-daylight period) have been selected to ensure $I2$ variations are independent of surface temperature changes.

A good agreement has been observed between both Aquarius and SMOS $I2$, and ice thickness variations over the four selected transects on East Antarctica, except for the case of fast spatial variations, which are better resolved by SMOS due to its higher spatial resolution. A linear trend has been observed between ice thickness changes and both Aquarius and SMOS $I2$ variations, with correlations of 0.6–0.7, and slopes of 8.6–9.5 K/km. As expected, no correlation has been found with the subglacial bedrock. Consistently with the maximum theoretical L-band penetration depth of 1–1.5 km, it does not contribute to be observed signal, being located, in general, ∼2–4.3 km below the ice surface. The presence of subglacial lakes may affect the vertical temperature profile and/or the dielectric properties of the ice layers above, affecting the observed $I2$.

This study could help in deciding future calibration/validation targets over Antarctica for upcoming L-band missions. Also, it could contribute to improve our understanding of the Antarctica's emissivity as a necessary step for the potential use of new L-band observations in cryosphere studies.

5. REFERENCES

[1] G. Macelloni *et al.*, "DOMEX 2004: An experimental campaign at Dome-C Antarctica for the calibration of spaceborne low-frequency microwave radiometers," *Geoscience and Remote Sensing, IEEE Transactions on*, vol. 44, no. 10, pp. 2642–2653, 2006.

[2] G. Macelloni *et al.*, "Ground-based L-Band emission measurements at Dome-C Antarctica: The DOMEX-2 experiment," *Geoscience and Remote Sensing, IEEE Transactions on*, vol. 51, no. 9, pp. 4718–4730, 2013.

[3] S.S. Kristensen *et al.*, "EMIRAD data: Presentation & Analysis, version 1.2," DOMECair Campaign, 2013.

[4] M. Pablos *et al.*, "SMOS and Aquarius radiometers: Intercomparison over selected targets," *Journal of Selected Topics in Applied Earth Observations and Remote Sensing, Special Issue of*, vol. 7, no. 9, pp. 3833–3844, 2014.

[5] P. Fretwell *et al.*, "Bedmap2: improved ice bed, surface and thickness datasets for Antarctica," *The Cryosphere*, vol. 7, no. 1, pp. 375–393, 2013.

[6] A. Wright and M. Siegert, "A fourth inventory of Antarctic subglacial lakes," *Antarctic Science*, vol. 24, no. 6, pp. 659–664, 2012.

[7] A. Sihvola and J.A. Kong, "Effective permittivity of dielectric mixtures," *Geoscience and Remote Sensing, IEEE Transactions on*, vol. 26, no. 4, pp. 420–429, 1988.

[8] M.A. Rist *et al.*, "Fracture of Antarctic shelf ice," *Journal of Geophysical Research: Solid Earth*, vol. 107, no. B1, pp. ECV2–1–ECV2–13, 2002.

[9] K.C. Jezek *et al.*, "Radiometric approach for estimating relative changes in intraglacier average temperature," *Geoscience and Remote Sensing, IEEE Transactions on*, vol. 52, no. 1, pp. 134–143, 2015.